LANGMUIR Article
Cite This: Langmuir 2017, 33, 12982-12988
pubs.acs.org/Langmuir

Switchable Surfactants for the Preparation of Monodisperse, Supported Nanoparticle Catalysts

Kristin Bryant, Gasim Ibrahim, and Steven R. Saunders*

The Gene and Linda Voiland School of Chemical Engineering and Bioengineering, Washington State University, Pullman, Washington 99164, United States

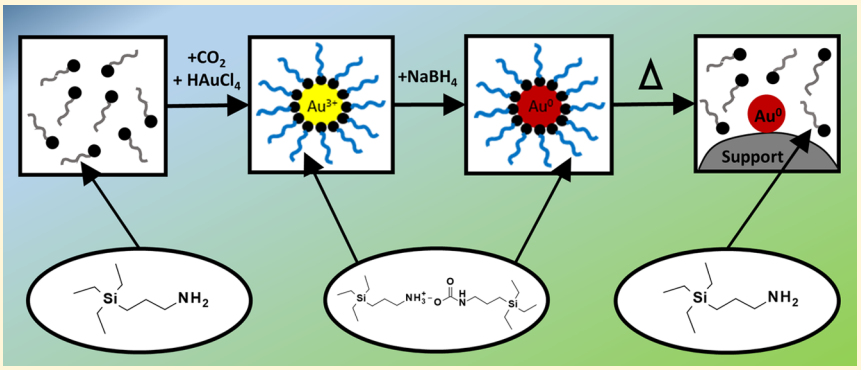

ABSTRACT: Synthesis methods for the preparation of monodisperse, supported nanoparticles remain problematic. Traditional synthesis methods require calcination following nanoparticle deposition to remove bound ligands and expose catalytic active sites. Calcination leads to significant and unpredictable growth of the nanoparticles resulting in polydisperse size populations. This undesired increase in nanoparticle size leads to a decrease in catalytic activity due to a loss of total surface area. In this work, we present the use of silylamines, a class of switchable solvents, for the preparation of monodisperse, supported nanoparticles. Silylamines are switchable molecules that convert between molecular and ionic forms by reaction with CO_2. Upon addition of an alkane, the switchable solvent behaves as a switchable surfactant (SwiS). The SwiS is used to template nanoparticles to aid in synthesis and subsequently used to release nanoparticles for deposition onto a support material. The use of SwiS allowed for the preservation of nanoparticle diameter throughout the deposition process. Finally, it is demonstrated that supported gold nanoparticle catalysts prepared using SwiS are up to 300% more active in the hydrogenation of 4-nitrophenol than their traditionally prepared analogues.

INTRODUCTION

Traditional synthetic methods of preparing supported nanoparticle catalysts typically require activation steps that significantly impact properties of the resulting catalyst, affecting characteristics such as size and shape and ultimately reduce catalytic activity of the nanoparticles on the catalyst support.[1−3] Precipitation and impregnation synthesis methods rely on physical processes that convert a metal precursor solution to a solid material followed by additional activation steps.[1,4] Precipitation often leaves the catalyst vulnerable to poisoning through the incomplete removal of anions during washing steps.[1] Additionally, impregnation methods generally lead to the formation of large and polydisperse nanoparticle populations.[5−7] In contrast to precipitation and impregnation methods, colloidal synthesis techniques have the advantage of nanoparticle size control via the use of stabilizing ligands. In many cases, nanoparticle size can be manipulated by varying ligand concentration[8−10] where increased concentrations of ligand inhibit nucleation and growth of the nanoparticle. After synthesis, the nanoparticles may be deposited onto a support material via methods similar to impregnation and precipitation. Calcination is required to remove the stabilizing ligands that block catalytic active sites prior to use. It has been reported in the literature that exposure of nanoparticles to elevated temperatures significantly increases nanoparticle size, resulting in decreased total surface area.[4,11−13] While chelating agents can be used to diminish or control the size change during calcination,[14] the inevitable size changes remain unpredictable. This unpredictability is not conducive to size-dependent studies or reactions that require fine control over nanoparticle size. Therefore, colloidal synthesis routes possess many of the same drawbacks as traditional heterogeneous catalyst synthesis techniques. Developing methods of supported nanoparticle synthesis and preparation in which nanoparticle size is finely controlled remains a nontrivial task. To our knowledge, a facile method for developing size-controlled, supported nanoparticle catalysts has yet to be established. In this study, we present the use of stabilizing ligands with switchable moieties, which offer novel strategies to avoid the drawbacks of calcination.

Received: August 23, 2017
Revised: October 20, 2017
Published: October 23, 2017

DOI: 10.1021/acs.langmuir.7b02983
Langmuir 2017, 33, 12982−12988

Switchable molecules are those that can undergo reversible structural changes in response to an external stimulus. One class of switchable solvents, termed reversible ionic liquids (RevIL), was originally designed for CO_2 sequestration.[15−17] In these systems, a silylamine molecular liquid (i.e., a nonionic liquid) can be converted to an ionic liquid by reaction with CO_2 forming ammonium−carbamate ion pairs (see Scheme 1).[15] It is accepted in the literature that the equilibrium reaction

Scheme 1. Reversible Reaction of a Silylamine Molecular Liquid with CO_2 To Form a Reversible Ionic Liquid

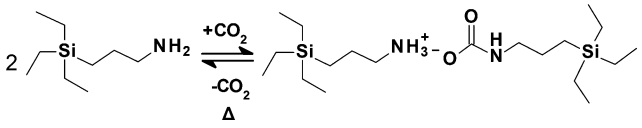

of CO_2 with a primary amine in traditional organic solvents produces a 2:1 amine to CO_2 mole ratio consisting of only ammonium and carbamate ion pairs.[18−22] Upon heating the ionic liquid to its unique reversal temperature, the CO_2 is released and the original amine is restored. The reversible nature of these liquids can be leveraged to prepare monodisperse nanoparticles as demonstrated by Ethier et al.[23] It is hypothesized that the mechanism behind the solubility of the gold precursor in the RevIL involves multiple equilibria that promote self-assembly of the reversible ionic surfactant through a reverse micelle formation during the synthesis of stabilized gold nanoparticles.[23−25] In this work, we demonstrate that RevIL dissolved in a hydrocarbon act as switchable surfactants (SwiS) to aid in the preparation of monodisperse nanoparticles and facilitate the deposition of surface-clean nanoparticles onto a catalyst support, eliminating the need for additional activation steps.

EXPERIMENTAL SECTION

Materials. Hydrogen tetrachloroaurate trihydrate ($HAuCl_4·3H_2O$; 49% Au), platinum(0)−1,3-divinyl-1,1,3,3-tetramethyldisiloxne (Pt−DVDS; ∼2% platinum), allylamine ($C_3H_5NH_2$; 98%), and triethylsilane ($C_6H_{16}Si$; 99%) were obtained from Sigma-Aldrich. Sodium borohydride ($NaBH_4$; >97%), 1-hexanol ($C_6H_{14}O$, 99%), and silica (SiO_2; 0.060−0.2 mm) were obtained from Alfa Aesar. 4-Nitrophenol ($C_6H_5NO_3$; 98%) and 1-dodecanethiol ($C_{12}H_{26}S$; 98%) were obtained from Acros Organics. Toluene (C_7H_8; >99.5%), *n*-hexane (C_6H_{14}; >95%), trisodium citrate ($Na_3C_6H_5O_7$; >99%), and hydrochloric acid (HCl; 36.5−38%) were obtained from J.T. Baker. Acetonitrile (C_2H_3N, HPLC grade) was obtained from Fisher Chemical. The 200 mesh carbon/formvar-coated copper grids were purchased from Ted Pella. Toluene was dried over molecular sieves for at least 24 h prior to use. All other materials were used without further purification.

Synthesis of 3-Aminopropyltriethylsilane Molecular Liquid. 3-Aminopropyltriethylsilane (APTES) is not commercially available and therefore was synthesized according to a literature procedure.[15] Triethylsilane (160 mmol, 1 equiv) and Pt−DVDS (1.6 mmol, 0.001 equiv) were mixed in a 250 mL round-bottom flask under nitrogen at room temperature. 80 mL of toluene was added to the reaction flask under magnetic stirring. The allylamine (320 mmol, 2 equiv) was added to the flask. The temperature was increased to 110 °C, and the reaction was allowed to proceed under refluxing toluene for 24 h. The conversion was monitored by ^{1}H NMR on a Bruker DRX 400. The crude product was then vacuum distilled at 3 Torr and 65 °C. The purified product was stored under dry nitrogen. ^{1}H NMR with $CDCl_3$ was used to confirm the structure and purity of APTES. ^{1}H NMR (400 Hz, $CDCl_3$), δ: 2.57 (t, 2H, $-C\underline{H}_2NH_2$), 1.33 (m, 2H, $-CH_2C\underline{H}_2CH_2$), 0.99 (s, 2H, $-N\underline{H}_2$), 0.84 (t, 9H, $-CH_2C\underline{H}_3$), 0.44 (t, 2H, $-C\underline{H}_2(CH_2)_2NH_2$), 0.41 (q, 6H, $-C\underline{H}_2Si$).

Reversible Ionic Liquid Formation. 4 mL of the synthesized APTES molecular liquid was added to a sealed and nitrogen purged vial containing a magnetic stir bar. The sample was sparged with CO_2 using a stainless steel needle to form the RevIL. The mass of the vial was measured every 10 min. Sparging was stopped when no mass change was seen for three consecutive measurements (∼3 h).

Switchable Surfactant-Stabilized Gold Nanoparticle Synthesis. Switchable surfactant (SwiS)-stabilized gold nanoparticles were synthesized using a modified version of a method available in the literature.[23] $HAuCl_4·3H_2O$ (0.0298 g; 0.076 mmol) was dissolved in the RevIL (3.9911 g; 0.010 mol). 17.6 mL of hexane was added to the vial. The resulting one-phase solution was mixed at 600 rpm until the $HAuCl_4$ was completely dissolved. 400 μL of a 0.1 M aqueous solution of $NaBH_4$ was added to the vial while stirring at 600 rpm. The resulting solution was stirred for 30 min to allow for complete reduction of the gold precursor. A small aliquot of the nanoparticle solution was diluted with hexane and deposited on a carbon/formvar-coated copper grid via drop-casting.

1-Dodecanethiol-Stabilized Gold Nanoparticle Synthesis. Trisodium citrate-stabilized gold nanoparticles were synthesized using a procedure available in the literature.[26] Stock solutions of 0.5 mM aqueous trisodium citrate and 0.5 mM gold chloride were prepared. 10 mL of each stock solution was added to a 25 mL round-bottom flask under magnetic stirring. 100 μL of 0.1 M aqueous $NaBH_4$ was added to the reaction flask. The solution was stirred at 500 rpm for 20 min.

The citrate-stabilized gold nanoparticles were phase-transferred into an organic phase for deposition onto the support. 10 mL of hexane containing 50 μL of 1-dodecanethiol was added to 20 mL of the nanoparticle solution in a round-bottom flask. 2 mL of HCl was added to the flask. The flask was capped and shaken vigorously for 1 min. The aqueous phase was removed and discarded. The remaining

Table 1. Deposition Conditions, Nanoparticle Sizes, Gold Loadings, and Gold Surface Atoms for All Catalyst Samples[a]

			supported nanoparticle diameter (nm)		gold loading (mg Au/g catalyst)		Au surface atoms/g catalyst × 10^{18}	
	deposition volume (mL hexane)	support mass (g SiO_2)	precalcination	postcalcination	precalcination	postcalcination	precalcination	postcalcination
SwiS-stabilized	52.5	1.5	3.3 ± 0.6	7.6 ± 2.5	0.157 ± 0.003	0.449 ± 0.003	61.1 ± 3.4	106.0 ± 1.9
	52.5	3	3.4 ± 0.5	5.6 ± 1.8	0.170 ± 0.004	0.398 ± 0.008	43.9 ± 1.6	132.6 ± 9.1
	102.5	1.5	3.3 ± 0.6	6.1 ± 1.7	0.266 ± 0.005	0.772 ± 0.004	57.6 ± 1.6	112.9 ± 3.2
	102.5	3	3.3 ± 0.7	6.1 ± 1.9	0.177 ± 0.004	0.475 ± 0.000	66.1 ± 2.2	109.1 ± 4.1
	152.5	1.5	3.3 ± 0.7	6.3 ± 1.9	0.226 ± 0.004	0.654 ± 0.017	46.6 ± 2.9	76.7 ± 2.3
	152.5	3	3.4 ± 0.6	5.6 ± 1.8	0.163 ± 0.003	0.368 ± 0.004	72.8 ± 3.7	75.6 ± 1.9
thiol-stabilized			3.7 ± 1.0	13.3 ± 7.1	0.050 ± 0.001	0.185 ± 0.003		25.7 ± 1.9

[a]Volume of the deposition solution was manipulated by addition of hexane. Diameter of the dispersed SwiS and thiol-stabilized nanoparticles was 3.4 ± 0.7 and 8.4 ± 2.3 nm, respectively.

DOI: 10.1021/acs.langmuir.7b02983
Langmuir 2017, 33, 12982−12988

organic phase containing the nanoparticles was washed with DI water three times. A small aliquot of the nanoparticle solution was diluted with hexane and deposited on a carbon/formvar-coated copper grid via drop-casting.

Nanoparticle Deposition. The SwiS-stabilized gold nanoparticles were deposited in six unique conditions. For each of the six conditions described in Table 1, 2.5 mL of the prepared nanoparticle solution was added to a 250 mL Erlenmeyer flask containing a large stir bar. Hexane (50, 100, or 150 mL) was added to the flask. Silica (1.5 or 3 g) was subsequently added to the flask. The mixtures were stirred at 400 rpm for the duration of the deposition process. The Erlenmeyer flasks were heated to reflux conditions (69 °C) and held for 30 min. The resulting solution was allowed to cool to room temperature. The colorless supernatant was removed and discarded. The remaining supported nanoparticles were thrice washed with 5 mL of hexane. The Erlenmeyer flasks containing the supported nanoparticles were placed in a vacuum oven set at 45 °C until the samples were dry.

The thiol-stabilized nanoparticles were deposited by adding 10 mL of nanoparticle solution to a 250 mL Erlenmeyer flask containing a large stir bar. 50 mL of hexane and 3 g of silica gel were added to the flask. The flask was heated to reflux conditions (69 °C) while stirring and held for 30 min before cooling to room temperature. The colorless supernatant was removed and discarded. The supported nanoparticles were thrice washed with 5 mL of hexane then placed in a vacuum oven set at 45 °C until dry.

Calcination. 0.5 g of each of the six samples was calcined in air in a furnace. The temperature was ramped at 5 °C/min to 500 °C from room temperature, held for 2 h, and then allowed to cool to room temperature.

Nanoparticle Characterization. Nanoparticle size was determined using transmission electron microscopy (TEM) utilizing an FEI Technai G2 T20 Twin TEM with an operating voltage of 200 kV. Samples were diluted in hexane and drop-cast onto 200 mesh carbon/formvar-coated copper grids. Image analysis was performed using ImageJ software. A minimum of 500 dispersed nanoparticles and 300 supported nanoparticles were manually sized for each sample by measuring the longest particle axis.

Dispersed nanoparticle concentrations and supported nanoparticle gold loadings were determined with inductively coupled plasma-mass spectroscopy (ICP-MS) utilizing an Agilent 7700 at the Peter Hooper GeoAnalytical Lab at Washington State University. A known mass of catalyst (or volume of dispersed nanoparticles) was digested in aqua regia and diluted to 2% HNO_3 for analysis.

Nanoparticle surface area was determined using a modified method available in the literature.[27] Chemisorption of 1-dodecanethiol was measured in order to determine the number of accessible gold surface atoms. For each sample, a known concentration (typically ~2.5 mM) solution of 1-dodecanethiol in acetonitrile (MeCN) was prepared. Roughly 200 mg of each catalyst sample and pure silica support were individually suspended in 3 mL of the 1-dodecanethiol solution and allowed to stir in a sealed flask for 24 h. The suspension was then quantitatively filtered through a syringe filter with a 0.2 μm nylon membrane into a 10 mL volumetric flask and the filter washed with approximately 6 mL of MeCN. 1-Hexanol was added to the volumetric flask as an internal standard such that the final concentration of 1-hexanol was 0.5 mM. The resulting solution was brought to 10 mL with MeCN to be analyzed with a gas chromatograph (GC) with a flame ionization detector. A ThermoFisher Trace 1300 GC was calibrated with six solutions of 1-dodecanethiol varying in concentration from 300 to 2000 μM, each containing 0.5 mM 1-hexanol. Filtrates of all samples were analyzed by GC to determine the concentration of 1-dodecanethiol that remained in solution after adsorption. The difference in 1-dodecanethiol concentration before and after filtration was assumed to be adsorbed on the gold surface (taking into account any 1-dodecanethiol potentially adsorbed on to the silica support).

Fourier transform infrared spectroscopy (FTIR) was used to characterize the catalyst surface as well as the molecular and ionic liquid utilizing a ThermoScientific Nicolet IS10. Spectra were collected from 650 to 4000 cm^{-1}.

Catalytic Activity Evaluation. The catalytic reduction of 4-nitrophenol was used to evaluate the activity of the catalyst samples (see Scheme 2). 16.8 mL of DI water was added to a 25 mL round-bottom flask with a magnetic stir bar. The contents of the flask were stirred at 500 rpm for the duration of the experiment. 0.6 mL of a 3 mM aqueous solution of 4-nitrophenol was added to the reaction flask followed by 0.6 mL of a 3 M aqueous solution of $NaBH_4$. The reaction solution rapidly turned bright yellow, indicating the formation of the 4-nitrophenolate ion. 1 mL of the reaction solution was transferred to a polystyrene cuvette with a 1 cm path length and then analyzed via UV−vis on an Agilent Cary Series 100. The absorbance value at 400 nm was taken as the initial absorbance of 4-nitrophenol. A known mass of catalyst sample (typically 0.05 g) was added to the reaction flask and a timer was immediately started. Samples were taken at 1 min intervals and immediately filtered through a syringe filter with a 0.2 μm nylon membrane for UV−vis analysis. Samples were taken until the reaction was complete, indicated by a color change from yellow to colorless. All activity tests were run in triplicate.

Scheme 2. Gold-Catalyzed Reduction of 4-Nitrophenol to 4-Aminophenol Proceeding through the 4-Nitrophenolate Intermediate

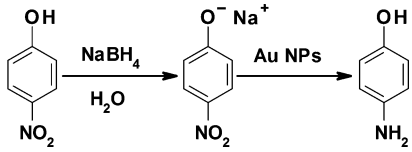

RESULTS AND DISCUSSION

The gold nanoparticles from a single synthesis batch were deposited in six unique conditions (e.g., varying mass of support and metal concentration) to allow for a range of dispersion of the nanoparticles across the support and then characterized to determine size distributions and catalytic activity. In this study, we focus only on APTES while other groups have previously considered the effect of silylamine alkyl chain length on nanoparticle size.[23] The deposition conditions are summarized in Table 1. For each deposition of SwiS-stabilized nanoparticles, approximately 0.83 mg of Au was present in solution. The catalysts synthesized with SwiS were compared to a traditionally prepared supported nanoparticle catalyst: thiol-stabilized gold nanoparticles from a modified Turkevich synthesis.[28]

Effect of Deposition on Nanoparticle Size. The average size of the synthesized dispersed thiol-stabilized nanoparticles was 8.4 ± 2.3 nm. After deposition, the average diameter decreased significantly to 3.7 ± 1.0 nm. We attribute this apparent decrease in average size to Ostwald ripening and thiol etching during the deposition process such that a small population of very large nanoparticles exists but is not accurately represented in the TEM analysis.

In contrast to the thiol-stabilized nanoparticles, we observe no statistically significant (determined by a single-factor ANOVA analysis and Tukey HSD[29] with $p > 0.05$ in all cases) change in nanoparticle size during deposition of the SwiS-stabilized nanoparticles in any of the conditions as shown in Table 1 and Figure 1. We note that this occurs at high gold loading values when compared to the thiol-stabilized nanoparticles. SwiS-stabilized nanoparticles maintain size throughout deposition to an extent that traditionally prepared nanoparticles cannot.

Effect of Calcination on Nanoparticle Size. Ligand-stabilized nanoparticles typically require a high-temperature

DOI: 10.1021/acs.langmuir.7b02983
Langmuir 2017, 33, 12982−12988

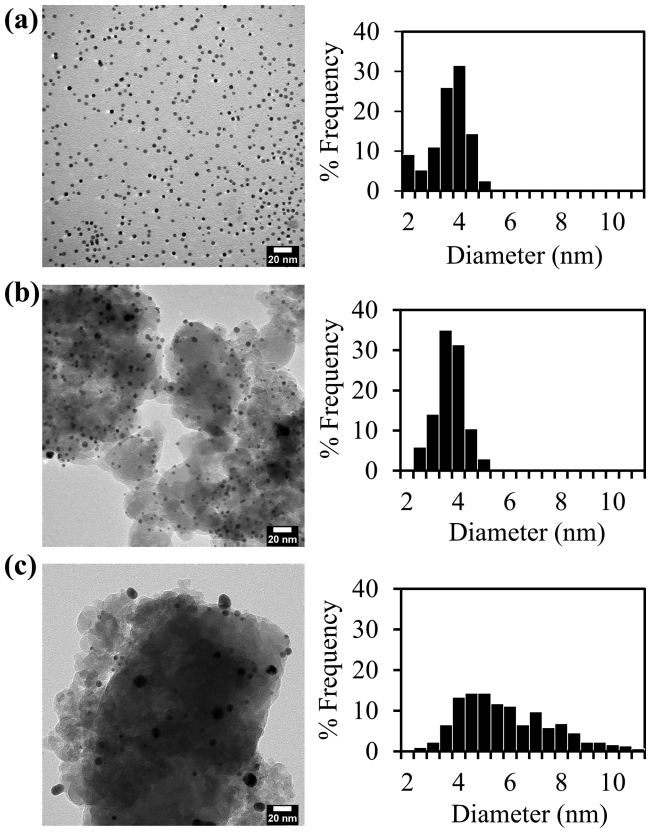

Figure 1. TEM micrographs and size distributions of a catalyst prepared with SwiS: (a) dispersed nanoparticles, (b) supported nanoparticles prior to calcination, and (c) supported nanoparticles after calcination. The catalyst was prepared with a deposition volume of 152.5 mL and 3 g of support.

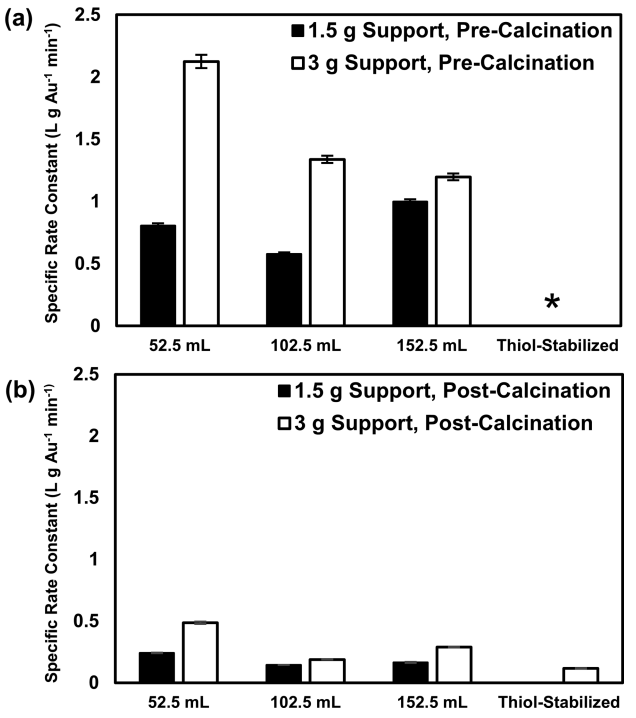

Figure 2. Specific rate constants of supported nanoparticle catalysts (a) before calcination and (b) after calcination. Asterisk (∗) indicates no observed catalytic activity.

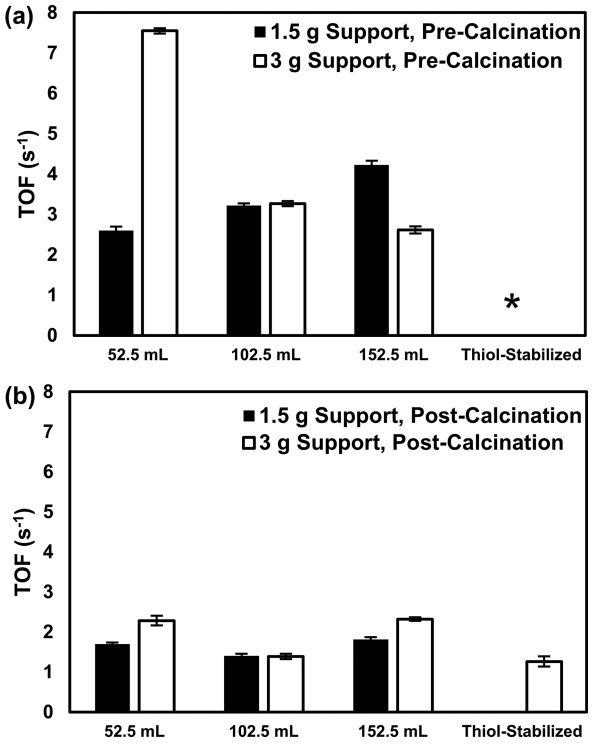

Figure 3. Turnover frequencies for all catalyst samples (a) before calcination and (b) after calcination. Asterisk (∗) indicates no observed catalytic activity.

calcination to remove the ligand and expose active sites.[30,31] As demonstrated in Figures 2 and 3, the thiol-stabilized nanoparticles used in this study were not catalytically active prior to calcination. While calcination is required to remove stabilizing ligands, this exposure to high temperatures significantly affects nanoparticle size. The size of the previously thiol-stabilized nanoparticles increased by approximately 260% from 3.7 ± 1.0 to 13.3 ± 7.1 nm due to calcination.

We hypothesize that the SwiS-stabilized dispersed nanoparticles are deposited onto the support via the reversal of the SwiS to molecular form and, thus, releasing from the surface of the nanoparticle. The size increase due to calcination in the SwiS samples was 130% (increasing from 3.3 ± 0.6 to 7.6 ± 2.5 nm) in the worst case and only 65% (increasing from 3.4 ± 0.6 to 5.6 ± 1.8 nm) in the best case. The diminished occurrence of nanoparticle growth in the SwiS samples indicates a more robust supported nanoparticle and one that is resistant to sintering. This resistance to sintering occurs even at relatively high catalyst loadings. Although comprehensive studies have not yet been completed, it is hypothesized that the diminished occurrence of sintering in catalysts prepared with SwiS is the result of the lack of a compressed ligand layer between the nanoparticle and support surface. The presence of the thiol ligand on the traditionally prepared catalyst increases the nanoparticle−support distance, leading to weak van der Waals interactions between the nanoparticle and support surface. During calcination, these weak van der Waals interactions allow for nanoparticle migration and agglomeration. In contrast, the reversal of the SwiS and the subsequent release of bare nanoparticles allows for direct deposition onto the support surface without a compressed ligand layer. As a result, stronger van der Waals attractions exist between the nanoparticles and

DOI: 10.1021/acs.langmuir.7b02983
Langmuir 2017, 33, 12982−12988

support surface, thus limiting the migration and agglomeration at high temperatures in SwiS-prepared samples.

Catalyst Loading. Gold loading values were calculated for all supported catalysts samples based on ICP-MS data collected before and after calcination. These values are displayed in Table 1. Prior to calcination, it was expected that the samples prepared with 3 g of support material would display roughly half the gold loading as the samples prepared with 1.5 g of support material. As displayed in Table 1, the catalysts generally follow the expected trend with the exception of the catalyst prepared with 1.5 g of support and a deposition volume of 52.5 mL. We see a significantly lower gold loading value than expected for this sample, which we attribute to either incomplete deposition of nanoparticles onto the support or deposition of nanoparticles on the glassware. After calcination, there is a significant increase in mass of gold per gram of catalyst, indicating the removal of water or other remaining species interacting with the catalyst surface. This observation is further addressed later using spectroscopic techniques.

Catalytic Activity. Apparent rate constants obtained from catalytic activity testing were converted to specific rate constants using gold loading values from ICP-MS and are shown in Figure 2. Specific rate constants are used as a measure of overall nanoparticle mass utilization. Prior to calcination, only the catalysts prepared with SwiS are catalytically active as the presence of the thiol ligand blocks active sites. The catalysts prepared with 3 g of support have higher specific rate constants than those prepared with 1.5 g of support in every case. We hypothesize that the enhanced rates of these samples are due to better dispersion of the nanoparticles across the surface of the support and decreased formation of multilayers of nanoparticles as the samples with 3 g of support provide greater deposition surface area. The SwiS sample with the highest specific rate (52.5 mL, 3 g) is approximately 60% more active than the next most active sample. Postcalcination, catalytic activity was observed in the thiol-prepared sample as stabilizing ligands were thermally degraded. The most catalytically active SwiS sample prior to calcination is approximately 300% more active than the catalyst prepared with thiol after calcination, indicating the presence of available active sites on the SwiS catalysts prior to calcination. In general, calcination significantly reduced the catalytic activity of the SwiS-prepared samples. The decrease in catalytic activity after calcination is a result of a loss of total nanoparticle surface area due to nanoparticle growth. Despite the reduction in activity, five of the six catalysts prepared with SwiS remained significantly more active than the catalyst prepared with the thiol. The catalyst with the highest specific rate after calcination is approximately 120% more active than the catalyst prepared with the thiol.

In order to obtain a better comparison of fundamental catalysis, specific rate constants were converted to turnover frequencies (TOF) before and after calcination by quantifying the surface area of gold on the catalyst samples. TOF is defined as

$$\mathrm{TOF} = \frac{n_{4\mathrm{NP}}}{n_{\mathrm{Au}} t}$$

where $n_{4\mathrm{NP}}$ is the number of moles of 4-nitrophenol consumed, n_{Au} is the moles of gold surface atoms (shown in Table 1), and t is the time of reaction. TOF for all samples are displayed in Figure 3. Similar to the specific rate constants, TOF of the SwiS samples prior to calcination are significantly higher than TOF after calcination in every case. The sample with the highest TOF (also the sample with the highest specific rate constant) is roughly 80% larger than the next highest sample. Additionally, the sample with the highest TOF is roughly 500% larger before calcination than the catalyst prepared with thiol after calcination. As is the case with the specific rate constants, every catalyst prepared with SwiS has a higher TOF than the catalyst prepared with thiol both before and after calcination, indicating the presence of sites that are fundamentally more active on the catalysts synthesized with SwiS. One would expect all of the TOF values prior to calcination to be relatively similar as the main contributing factor to TOF variability is nanoparticle size: larger nanoparticles typically possess a decreased fundamental catalytic activity.[32] Considering every catalyst sample exhibits the same average nanoparticle size prior to calcination, very little site-to-site variability was expected. The underlying reasons for this phenomenon are unclear without further investigation.

An interesting trend is seen in the number of surface atoms/g catalyst before vs after calcination as shown in Table 1. It was expected that the number of Au surface atoms would decrease after calcination due to an increase in average nanoparticle size; however, the opposite is seen. While nanoparticle size does increase, the number of Au surface atoms also increases while TOF decreases. This shows further evidence that an unknown species is possibly interacting with the surface of the catalyst and blocking active sites prior to calcination. However, the fact that TOF decreases after calcination implies that the catalysts are significantly more active prior to calcination even with a species potentially blocking active sites.

FTIR was used to address the presence of unknown species on the surface of the SwiS catalysts prior to calcination. FTIR spectra of all synthesis components are shown in Figure 4. The molecular liquid is evidenced by the CH_2 peak at 2900 cm^{-1} and the N−H stretching band at 3250−3370 cm^{-1}. A CH_2 peak is again seen in the ionic liquid spectrum; however, the presence of the ionic species is characterized by a shift in the N−H stretching band at 2600−3100 cm^{-1}, corresponding to the ammonium cation as well as the presence of the asymmetric CO_2^- stretch of the carbamate anion at 1575 cm^{-1}.[17] The dispersed SwiS nanoparticles are stabilized by only ionic liquid, as the N−H stretch of the molecular species is absent. The supported nanoparticles exhibit the CH_2 peak as well as the characteristic N−H stretching band of the molecular liquid at a relatively low intensity. It has been shown in the literature that when the amine is chemically bound to Au nanoparticles, there is a complete disappearance of this characteristic N−H stretch.[33] Thus, the presence of these peaks indicates that unbound molecular liquid interacts with the catalyst surface postdeposition. Pure silica support was subjected to the deposition process in the absence of nanoparticles to further investigate how the molecular liquid interacts with the catalyst surface. The synthesis and deposition process was repeated without the addition of the gold precursor nor $NaBH_4$. The FTIR spectrum of the "silica deposition" indicates that molecular liquid wets the surface of the support even after deposition and washing. While we can conclude that molecular liquid interacts with the support surface postdeposition, it remains unclear if the molecular liquid interacts with the gold surface as well. A complete absence of the N−H stretch band between 3250 and 3370 cm^{-1} is required to confirm that there is any molecular liquid bound to the nanoparticle surface postdeposition. In comparing the deposited silica with the as-purchased silica, we see a broad peak associated with water

DOI: 10.1021/acs.langmuir.7b02983
Langmuir 2017, 33, 12982−12988

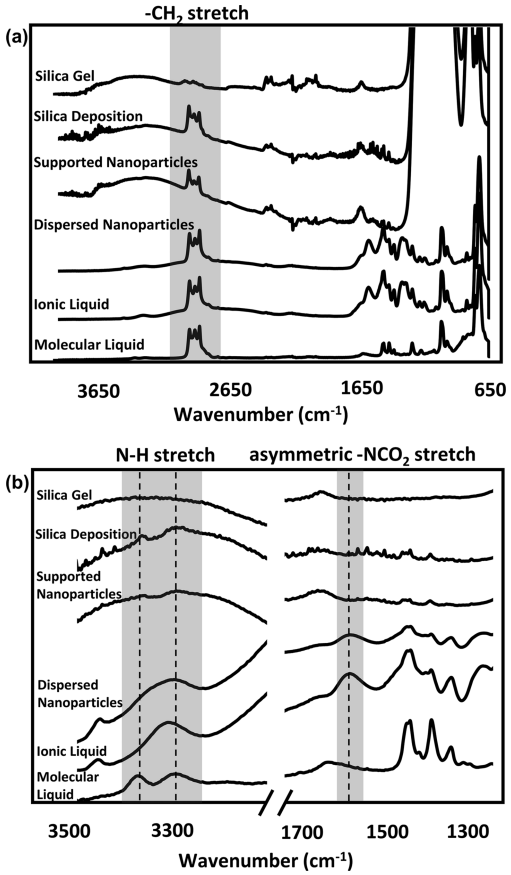

Figure 4. FTIR spectra of all synthesis components for supported nanoparticle catalysts prepared with SwiS. The wavenumber axis is broken from 1700 to 3100 cm^{-1} in (b).

from 3100 to 3500 cm^{-1} in both spectra. We suspect that the large water peak, which overlaps with the N−H stretch region of the molecular liquid, is responsible for an underrepresentation of the intensity of the N−H stretch of the molecular liquid in the supported nanoparticle sample, providing further evidence of the presence of the unbound species. This supports the hypothesis that the actual number of active sites is larger than that determined by the 1-dodecanethiol adsorption studies. While some molecular liquid does remain on the catalyst surface after nanoparticle deposition, it does not impede catalysis by completely blocking active sites.

CONCLUSIONS

A facile method to utilize the reversible nature of silylamines to prepare and deposit relatively surface-clean nanoparticles onto a support material while preserving nanoparticle size has been demonstrated. Supported nanoparticle catalysts prepared with SwiS do not require calcination as after the RevIL is reversed during deposition, a highly active catalyst with minimal or no other species bound to the surface of the nanoparticle is formed. Additionally, we have shown calcination leads to increased nanoparticle size and thus a loss of total surface area for catalysis. Calcination results in nanoparticle growth in every case; however, nanoparticles prepared with SwiS are significantly more resistant to sintering. Even after calcination, nanoparticles prepared with SwiS are superior to supported nanoparticle catalysts prepared via traditional methods.

AUTHOR INFORMATION

Corresponding Author

*E-mail steven.r.saunders@wsu.edu; Ph 509-335-6578 (S.R.S.).

ORCID

Steven R. Saunders: 0000-0001-6714-7435

Notes

The authors declare no competing financial interest.

ACKNOWLEDGMENTS

This work was supported by the National Science Foundation under CBET-1651597, institutional funding from Washington State University, and the Fulbright Foreign Student Scholar program. The authors thank the Franceschi Microscopy & Imaging Center and the Washington State University Center for NMR Spectroscopy for access to resources.

ABBREVIATIONS

RevIL, reversible ionic liquid; SwiS, switchable surfactant; APTES, 3-aminopropyltriethylsilane.

REFERENCES

(1) Munnik, P.; de Jongh, P. E.; de Jong, K. P. Recent Developments in the Synthesis of Supported Catalysts. *Chem. Rev.* **2015**, *115*, 6687−6718.

(2) Neimark, A.; Kheifets, L.; Fenelonov, V. Theory of Preparation of Supported Catalysts. *Ind. Eng. Chem. Prod. Res. Dev.* **1981**, *20*, 439−450.

(3) Lekhal, A.; Glasser, B. J.; Khinast, J. G. Impact of Drying on the Catalyst Profile in Supported Impregnation Catalysts. *Chem. Eng. Sci.* **2001**, *56* (15), 4473−4487.

(4) Schwarz, J. A.; Contescu, C.; Contescu, A. Methods for Preparation of Catalytic Materials. *Chem. Rev.* **1995**, *95* (3), 477−510.

(5) Delannoy, L.; El Hassan, N.; Musi, A.; Le To, N. N.; Krafft, J. M.; Louis, C. Preparation of Supported Gold Nanoparticles by a Modified Incipient Wetness Impregnation Method. *J. Phys. Chem. B* **2006**, *110* (45), 22471−22478.

(6) Hutchings, G. J. Catalysis by Gold. *Catal. Today* **2005**, *100* (1−2), 55−61.

(7) Kozlova, A. P.; Kozlov, A. I.; Sugiyama, S.; Matsui, Y.; Asakura, K.; Iwasawa, Y. Study of Gold Species in Iron-Oxide-Supported Gold Catalysts Derived from Gold-Phosphine Complex Au(PPh3)(NO3) and As-Precipitated Wet $Fe(OH)_3$*. *J. Catal.* **1999**, *181* (1), 37−48.

(8) Teranishi, T.; Miyake, M. Size Control of Palladium Nanoparticles and Their Crystal Structures. *Chem. Mater.* **1998**, *10* (2), 594−600.

(9) Hussain, I.; Graham, S.; Wang, Z.; Tan, B.; Sherrington, D. C.; Rannard, S. P.; Cooper, A. I.; Brust, M. Size-Controlled Synthesis of Near-Monodisperse Gold Nanoparticles in the 1−4 Nm Range Using Polymeric Stabilizers. *J. Am. Chem. Soc.* **2005**, *127*, 16398−16399.

(10) Aslam, M.; Fu, L.; Su, M.; Vijayamohanan, K.; Dravid, V. P. Novel One-Step Synthesis of Amine-Stabilized Aqueous Colloidal Gold Nanoparticles. *J. Mater. Chem.* **2004**, *14*, 1795−1797.

(11) Fujihara, S.; Maeda, T.; Ohgi, H.; Hosono, E.; Imai, H.; Kim, S. Hydrothermal Routes To Prepare Nanocrystalline Mesoporous SnO_2 Having High Thermal Stability. *Langmuir* **2004**, *20* (15), 6476−6481.

(12) Liang, Y.; Fan, J.; Xia, X.; Jia, Z. Synthesis and Characterisation of SnO_2 Nano-Single Crystals as Anode Materials for Lithium-Ion Batteries. *Mater. Lett.* **2007**, *61* (22), 4370−4373.

(13) Kayani, Z. N.; Saleemi, F.; Batool, I. Effect of Calcination Temperature on the Properties of ZnO Nanoparticles. *Appl. Phys. A: Mater. Sci. Process.* **2015**, *119* (2), 713−720.

(14) Koizumi, N.; Ibi, Y.; Hongo, D.; Hamabe, Y.; Suzuki, S.; Hayasaka, Y.; Shindo, T.; Yamada, M. Mechanistic Aspects of the Role of Chelating Agents in Enhancing Fischer − Tropsch Synthesis Activity of Co/SiO_2 Catalyst: Importance of Specific Interaction of Co

DOI: 10.1021/acs.langmuir.7b02983
Langmuir 2017, 33, 12982−12988

with Chelate Complex during Calcination. *J. Catal.* **2012**, *289*, 151−163.
(15) Rohan, A. L.; Switzer, J. R.; Flack, K. M.; Hart, R. J.; Sivaswamy, S.; Biddinger, E. J.; Talreja, M.; Verma, M.; Faltermeier, S.; Nielsen, P. T.; Pollet, P.; Schuette, G. F.; Eckert, C. A.; Liotta, C. L. The Synthesis and the Chemical and Physical Properties of Non-Aqueous Silylamine Solvents for Carbon Dioxide Capture. *ChemSusChem* **2012**, *5* (11), 2181−2187.
(16) Jessop, P. G.; Heldebrant, D. J.; Li, X.; Eckert, C. A.; Liotta, C. L. Green Chemistry: Reversible Nonpolar-to-Polar Solvent. *Nature* **2005**, *436*, 1102.
(17) Switzer, J. R.; Ethier, A. L.; Flack, K. M.; Biddinger, E. J.; Gelbaum, L.; Pollet, P.; Eckert, C. A.; Liotta, C. L. Reversible Ionic Liquid Stabilized Carbamic Acids: A Pathway Toward Enhanced CO_2 Capture. *Ind. Eng. Chem. Res.* **2013**, *52* (36), 13159−13163.
(18) Versteeg, G. F.; Van Dijck, L. A. J.; Van Swaaij, W. P. M. On the Kinetics Between CO_2 and Alkanolamines Both in Aqueous and Non-Aqueous Solutions. An Overview. *Chem. Eng. Commun.* **1996**, *144*, 113−158.
(19) Crooks, J. E.; Donnellan, J. P. Kinetics and Mechanism of the Reaction between Carbon Dioxide and Amines in Aqueous Solution. *J. Chem. Soc., Perkin Trans. 2* **1989**, 331−333.
(20) Caplow, M. Kinetics of Carbamate Formation and Breakdown. *J. Am. Chem. Soc.* **1968**, *90* (24), 6795−6803.
(21) Danckwerts, P. V. The Reaction of CO_2 with Ethanolamines. *Chem. Eng. Sci.* **1979**, *34* (4), 443−446.
(22) Wright, H. B.; Moore, M. B. Reactions of Aralkyl Amines with Carbon Dioxide. *J. Am. Chem. Soc.* **1948**, *70*, 3865−3866.
(23) Ethier, A. L.; Hart, E. C.; Saunders, S. R.; Biddinger, E. J.; Fadhel, A. Z.; Dilek, C.; Pollet, P.; Eckert, C. A.; Liotta, C. L. Reversible Ionic Surfactants for Gold Nanoparticle Synthesis. *Green Mater.* **2014**, *2* (2), 54−61.
(24) Eastoe, J.; Hollamby, M. J.; Hudson, L. Recent Advances in Nanoparticle Synthesis with Reversed Micelles. *Adv. Colloid Interface Sci.* **2006**, *128−130*, 5−15.
(25) Porta, F.; Krpetic, Z.; Prati, L.; Gaiassi, A.; Scarı, G. Gold-Ligand Interaction Studies of Water-Soluble Aminoalcohol Capped Gold Nanoparticles by NMR. *Langmuir* **2008**, *24* (14), 7061−7064.
(26) Jana, N. R.; Gearheart, L.; Murphy, C. J. Seeding Growth for Size Control of 5−40 Nm Diameter Gold Nanoparticles. *Langmuir* **2001**, *17* (22), 6782−6786.
(27) Janz, A.; Köckritz, A.; Yao, L.; Martin, A. Fundamental Calculations on the Surface Area Determination of Supported Gold Nanoparticles by Alkanethiol Adsorption. *Langmuir* **2010**, *26* (9), 6783−6789.
(28) Turkevich, J.; Stevenson, P. C.; Hillier, J. A Study of the Nucleation and Growth Processes in the Synthesis of Colloidal Gold. *Discuss. Faraday Soc.* **1951**, *11*, 55−75.
(29) Tukey, J. W. *Exploratory Data Analysis* **1977**, 5−24.
(30) Grunwaldt, J.; Kiener, C.; Wogerbauer, C.; Baiker, A. Preparation of Supported Gold Catalysts for Low-Temperature CO Oxidation via " Size-Controlled " Gold Colloids. *J. Catal.* **1999**, *181*, 223−232.
(31) Grunwaldt, J.; Maciejewski, M.; Becker, O. S.; Fabrizioli, P.; Baiker, A. Comparative Study of Au/TiO_2 and Au/ZrO2 Catalysts for Low-Temperature CO Oxidation. *J. Catal.* **1999**, *186*, 458−469.
(32) Panigrahi, S.; Basu, S.; Praharaj, S.; Pande, S.; Jana, S.; Pal, A.; Ghosh, S. K.; Pal, T. Synthesis and Size-Selective Catalysis by Supported Gold Nanoparticles: Study on Heterogeneous and Homogeneous Catalytic Process. *J. Phys. Chem. C* **2007**, *111* (12), 4596−4605.
(33) Yang, G.; Chang, W.; Hallinan, D. T. A Convenient Phase Transfer Protocol to Functionalize Gold Nanoparticles with Short Alkylamine Ligands. *J. Colloid Interface Sci.* **2015**, *460*, 164−172.

DOI: 10.1021/acs.langmuir.7b02983
Langmuir 2017, 33, 12982−12988